

## Atmospheric wet and dry deposition of dissolved inorganic nitrogen to the South China Sea

[Ying GAO](#), [Lifang WANG](#), [Xianghui GUO](#), [Yi XU](#) and [Li LUO](#)

Citation: [SCIENCE CHINA Earth Sciences](#); doi: 10.1007/s11430-019-9612-2

View online: <http://engine.scichina.com/doi/10.1007/s11430-019-9612-2>

Published by the [Science China Press](#)

---

### Articles you may be interested in

[Deep water bottom current deposition in the northern South China Sea](#)

Science in China Series D-Earth Sciences **50**, 1060 (2007);

[Estimation of dry deposition fluxes of major inorganic species by canopy throughfall approach](#)

Chinese Science Bulletin **51**, 1818 (2006);

[Paleogene marine deposition records of rifting and breakup of the South China Sea: An overview](#)

SCIENCE CHINA Earth Sciences **60**, 2128 (2017);

[Coral reef ecosystems in the South China Sea as a source of atmospheric CO<sub>2</sub> in summer](#)

Chinese Science Bulletin **56**, 676 (2011);

[Statistical estimations of atmospheric duct over the South China Sea and the Tropical Eastern Indian Ocean](#)

Chinese Science Bulletin **58**, 2794 (2013);

---

# Atmospheric wet and dry deposition of dissolved inorganic nitrogen to the South China Sea

Ying GAO<sup>1,2</sup>, Lifang WANG<sup>1,2</sup>, Xianghui GUO<sup>1,2,3\*</sup>, Yi XU<sup>1</sup> & Li LUO<sup>4</sup>

<sup>1</sup> State Key Laboratory of Marine Environmental Science, Xiamen University, Xiamen 361102, China;

<sup>2</sup> College of Ocean and Earth Sciences, Xiamen University, Xiamen 361102, China;

<sup>3</sup> Fujian Provincial Key Laboratory for Coastal Ecology and Environmental Studies, Xiamen University, Xiamen 361102, China;

<sup>4</sup> Jiangxi Provincial Key Laboratory for Causes and Control of Atmospheric Pollution, East China University of Technology, Nanchang 330013, China

Received December 6, 2019; revised March 2, 2020; accepted April 15, 2020; published online June 29, 2020

**Abstract** At the global scale, atmospheric inputs of nitrogen are an important source of the new nitrogen that supports new marine production, especially in oligotrophic open oceans and marginal seas. This study reports quantities of atmospheric deposition of dissolved inorganic nitrogen (DIN) to the largest marginal sea in the North Pacific (the oligotrophic South China Sea, SCS) based primarily on rainwater sampling in the open northwestern region (Yongxing Island) from 2013 to 2015, and aerosol sampling from the SCS basin in June 2017. Atmospheric wet and dry deposition of DIN and their potential contributions to productivity were estimated. The volume-weighted mean rainwater concentrations during the wet and dry seasons were 4.9 and 18.1  $\mu\text{mol L}^{-1}$  for N+N ( $\text{NO}_3^- + \text{NO}_2^-$ ), and 5.7 and 4.0  $\mu\text{mol L}^{-1}$  for  $\text{NH}_4^+$ , respectively. Rainwater concentrations of DIN were lower in the marginal seas than in the open ocean. The aerosol  $\text{NO}_3^-$  concentration was  $1.15 \pm 1.18 \mu\text{g m}^{-3}$  during the wet season, which is slightly lower than reported for the East China Sea and East Sea, but higher than in the Arabian Sea. Monthly wet and dry deposition rates ranged from 0.4–3.9 and 0.4–1.2  $\text{mmol m}^{-2} \text{mon}^{-1}$  for  $\text{NO}_3^-$ , and 0.2–1.3 and 0.01–0.02  $\text{mmol m}^{-2} \text{mon}^{-1}$  for  $\text{NH}_4^+$ , respectively. The annual wet and dry deposition fluxes of DIN were estimated to be 16.8 and 10.1  $\text{mmol m}^{-2} \text{yr}^{-1}$ , respectively. Compared to other marginal seas, the SCS receives less atmospheric  $\text{NO}_3^-$  inputs than the Yellow Sea, East China Sea, East Sea, and northeastern Mediterranean Sea. The total atmospheric DIN deposition may account for 1.8–11.1% of the nitrogen supporting new production and 0.7–1.8% of the nitrogen supporting primary production.

**Keywords** South China Sea, Atmospheric deposition, Wet deposition, Dry deposition, Nitrate,  $\text{NO}_3^-$ , Ammonium,  $\text{NH}_4^+$

**Citation:** Gao Y, Wang L, Guo X, Xu Y, Luo L. 2020. Atmospheric wet and dry deposition of dissolved inorganic nitrogen to the South China Sea. *Science China Earth Sciences*, 63, <https://doi.org/10.1007/s11430-019-9612-2>

## 1. Introduction

Nutrients are necessary elements to support marine primary production, which is the base of the ocean's ecosystems. The macronutrients include nitrogen (N), phosphate (P) and silicate (Si) (Millero, 2016). Generally, the nutrients are assimilated at a N:P:Si ratio of 16:1:16, which is the classic

Redfield ratio (Redfield et al., 1963). The insufficient element to support assimilation at this ratio is defined as the limiting element for primary production. In the upper layer (euphotic zone) of the oligotrophic oceans, such as the North Pacific Ocean, N is generally the limiting element (Krishnamurthy et al., 2007).

Reactive nitrogen ( $\text{N}_r$ ) includes all forms of N that are biologically, photochemically and/or radiatively active, including inorganic oxidized N (e.g.,  $\text{NO}_x$ ,  $\text{NO}_3^-$ ,  $\text{HNO}_3$ ,  $\text{N}_2\text{O}$ ),

\* Corresponding author (email: [xhguo@xmu.edu.cn](mailto:xhguo@xmu.edu.cn))

inorganic reduced species (e.g.,  $\text{NH}_4^+$ ,  $\text{NH}_3$ ) and N in organic compounds (Duce et al., 1991; Fowler et al., 2013; Galloway and Cowling, 2002). Atmospheric deposition is an important source of new N to the euphotic zone (Duce, 1986), and along with riverine inputs, nitrogen fixation, upward advection and diffusion and horizontal transport, supports new production (Chen et al., 2001; Karl, 1999; Prospero et al., 1996). In oligotrophic marginal seas, the contribution from atmospheric deposition can be extremely important, especially in spring and summer when the water column is stratified (Jickells and Spokes, 2001; Zhang J J et al., 2019). In the East Sea, the total atmospheric deposition rate (both wet and dry) of DIN (dissolved inorganic nitrogen, including  $\text{NO}_3^-$ ,  $\text{NO}_2^-$  and  $\text{NH}_4^+$ ) was recently estimated as  $\sim 175 \mu\text{mol N m}^{-2} \text{d}^{-1}$  (Park et al., 2019), larger than the  $\text{N}_2$  fixation rate ( $29.3\text{--}152 \mu\text{mol N m}^{-2} \text{d}^{-1}$ , Shiozaki et al., 2009). In the Mediterranean Sea, the total atmospheric dissolved nitrogen (DN, including DIN and dissolved organic nitrogen, DON) deposition rate was estimated to be  $0.092 \text{Tmol N yr}^{-1}$  (Kanakidou et al., 2020), which is larger than the maximum riverine input ( $0.079 \text{Tmol N yr}^{-1}$ ) and wastewater discharge from coastal cities ( $0.019 \text{Tmol N yr}^{-1}$ , Ludwig et al., 2009).

Atmospheric inputs have a significant effect on the ocean's chemistry and ecosystems (Boreddy and Kawamura, 2015). At the global scale, total net  $\text{N}_r$  deposition to the ocean was  $\sim 4.8 \text{Tmol N yr}^{-1}$  in 2000, comparable to the rate of marine  $\text{N}_2$  fixation ( $\sim 7.1 \text{Tmol N yr}^{-1}$ , and supported  $\sim 3.5\%$  of new production (Dentener et al., 2006; Duce et al., 2008). In the northern SCS, the atmospheric deposition of  $\text{N}_r$  supports  $5.6\text{--}8.7\%$  of primary production (Chen and Huang, 2018). In the East China Sea, the total atmospheric deposition of DIN supports  $1.1\text{--}3.9\%$  of the primary production (Zhang et al., 2010). In the Yellow Sea, the total atmospheric DN deposition supports  $0.3\text{--}6.7\%$  of the primary production (Qi et al., 2013). The atmospheric deposition of DIN supports  $\sim 2.4\%$  and  $\sim 1.9\%$  of the primary production in the coastal areas east of the Korean Peninsula and in the East Asian marginal seas, respectively (Park et al., 2019).  $\text{NO}_x$  and  $\text{NH}_y$  account for  $\sim 26.3\%$  of the globally external supply, supporting  $\sim 0.5\%$  of primary production and  $\sim 2.3\%$  of new production in the global ocean (Duce et al., 2008; Ducklow, 1995; Laws et al., 2000; Oschlies, 2001).

The South China Sea (SCS) is the largest marginal sea (approximately  $3.5 \times 10^6 \text{ km}^2$ ) of the North Pacific Ocean, with typical oligotrophic features (Shi et al., 2010; Wong et al., 2007). The SCS is located at the center of the Asian-Australian monsoon system and joins the subtropical East Asian monsoon, the tropical Indian monsoon, the western North Pacific monsoon, and the Australian monsoon (Wang et al., 2009). The SCS receives polluted air masses from East Asia in autumn and winter, and from Southeast Asia in

spring and summer (Atwood et al., 2013; Geng et al., 2019; Song et al., 2018; Xiao et al., 2017), influenced by the emissions from nearby developing countries and regions such as China, Thailand, Vietnam, Indonesia, Malaysia and the Philippines. Besides atmospheric deposition, the SCS also receives riverine inputs from the Mekong River, the Pearl River, the Red River and the Hanjiang River, as well as others. Based on the Acid Deposition Monitoring Network in East Asia (EANET), the input of atmospheric  $\text{N}_r$  to the SCS was estimated to be  $\sim 55 \text{ mmol N m}^{-2} \text{ yr}^{-1}$  (Kim et al., 2014). Nevertheless, studies of DIN deposition to the SCS based on filed observations are limited, and include studies from Dongsha Island on the northern SCS shelf and coastal Daya Bay (Chen and Huang, 2018; Wu et al., 2018; Yang et al., 2014). However, atmospheric DIN deposition estimates based on field observations in the open SCS are scarce, and may be a critical, under-examined aspect of the N cycle given the oligotrophic character of the open SCS.

In this study, we report  $\text{NO}_3^-$  plus  $\text{NO}_2^-$  (N+N) and  $\text{NH}_4^+$  concentrations in rainwater,  $\text{NO}_3^-$  in atmospheric aerosols, and evaluate DIN deposition fluxes primarily based on observations from Yongxing Island in the open northwestern SCS, and from the northern and middle SCS onboard the R/V Tan Kah Kee (TKK). The importance of atmospheric DIN deposition to productivity in the oligotrophic SCS will also be discussed.

## 2. Materials and methods

### 2.1 Rainwater and aerosol sample collection

Forty rainwater samples were collected from Yongxing Island (Figure 1) in September 2013, from May 2014 to January 2015, and in April 2015. Samples were collected in clean plastic buckets and stored in 120 mL high-density polyethylene bottles (Nalgene) at  $-20^\circ\text{C}$  until analysis. Among all the samples, 1 was collected in September 2013, 37 were collected from May 2014 to January 2015, and the remaining 2 samples were collected in April 2015. The rainwater sampling duration was  $0.2\text{--}24.3 \text{ h}$  for each sample.

Twenty-two aerosol samples were collected over the SCS from June 5–27, 2017, during the process study cruise of project CHOICE-C II (Carbon cycling in China Seas-budget, controls and ocean acidification II) (Figure 1). Aerosol samples were taken using a Laoying® 2031 large-volume total suspended aerosol particle sampler through a Whatman™ quartz microfiber filter ( $203 \text{ mm} \times 254 \text{ mm}$  QMA filters) at a speed of  $\sim 1.05 \text{ m}^3 \text{ min}^{-1}$ . Aerosol sampling duration was  $8.7\text{--}40.8 \text{ h}$  for each sample. All samples were stored in a refrigerator at  $-20^\circ\text{C}$  until analysis. Wind speed and direction were measured and recorded by a Vaisala AWS430 automatic weather station. The precision was  $0.3 \text{ m s}^{-1}$  for wind speed and  $3^\circ$  for wind direction.

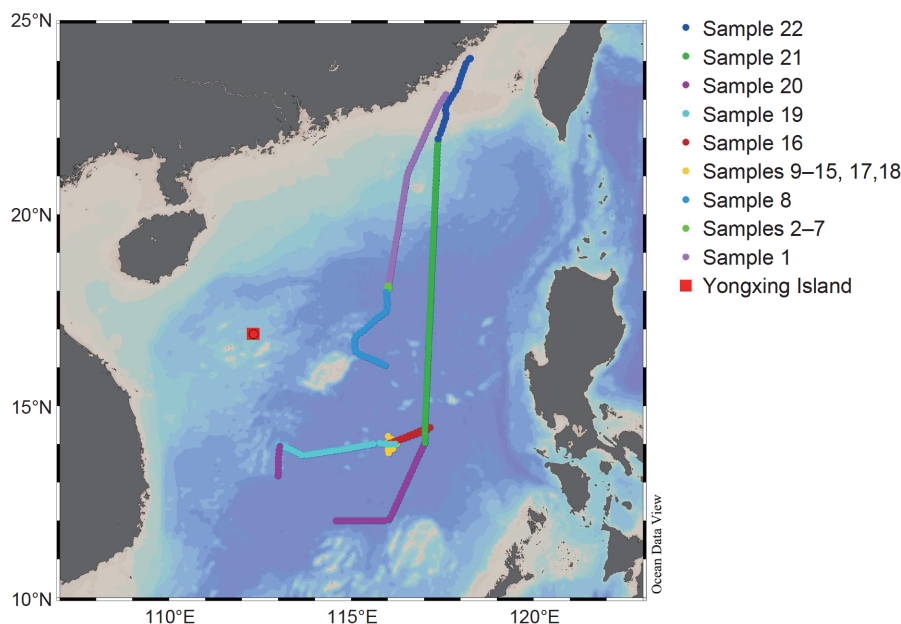


**Figure 1** Map of the South China Sea with sampling sites and the aerosol sampling track. The red square represents Yongxing Island, where the rainwater samples were collected. The colored lines and dots show the locations where the aerosol samples were taken, with close stations indicated by the same color.

## 2.2 Chemical analysis

Total  $\text{NO}_3^- + \text{NO}_2^-$  concentrations in rainwater samples were measured via a spectrophotometric method using a Bran+Luebbe AA3 auto analyzer (Technicon Auto-Analyzer III). The detection limits of  $\text{NO}_2^-$  and  $\text{NO}_3^-$  were 0.04 and 0.10  $\mu\text{mol L}^{-1}$  (Han et al., 2012), respectively.  $\text{NH}_4^+$  concentrations in rainwater samples were measured using an indophenol blue method with a detection limit of 0.1  $\mu\text{mol L}^{-1}$  (Pai et al., 2001).

For the aerosol samples, an eighth of each aerosol filter was extracted with 50 mL of Milli-Q water (conductivity 18.2  $\text{m}\Omega \text{cm}^{-1}$ ) in a clean centrifuge tube, and ultrasonically oscillated for 30 min. The extracts were then filtered using 0.22  $\mu\text{m}$  Millipore syringe filters. The concentration of  $\text{NO}_3^-$  was analyzed by ion chromatography using a Dionex-AQUION ICS-1100 ion chromatograph (Thermo Fisher Scientific, Inc., USA) equipped with a DS6 heated conductivity cell. The precision of  $\text{NO}_3^-$  measurements was better than 5%. As aerosol nitrite ( $\text{NO}_2^-$ ) concentrations are generally below the detection limit (Hsu et al., 2014; Luo et al., 2016), we use aerosol  $\text{NO}_3^-$  concentrations to represent aerosol N+N concentrations in this study.

## 2.3 Back trajectory analysis

The Hybrid Single-Particle Lagrangian Integrated Trajectory (HYSPPLIT) Model based on available Global Data Assimilation System (GDAS) wind data was used for illustrating the possible air mass trajectories (NOAA Air Resources

Laboratory, <http://ready.arl.noaa.gov/HYSPLIT.php>). For each sample, 72 h back trajectories of air masses were computed, with the levels of the model set to 200, 500 and 1000 m.

## 2.4 Wet and dry deposition flux estimates

### 2.4.1 Wet deposition estimates

The wet deposition flux of N+N or  $\text{NH}_4^+$  is the product of the volume-weighted mean (VWM) concentration of N+N or  $\text{NH}_4^+$  and the amount of precipitation, calculated using eqs. (1) and (2) (Baker et al., 2010; Duce et al., 1991; Spokes et al., 2000; Wang et al., 2018; Xing et al., 2017; Zhang X et al., 2019):

$$C_{\text{VWM}} = \frac{\sum_{i=1}^n C_i P_i / \sum_{i=1}^n P_i}{\sum_{i=1}^n P_i} \quad (1)$$

$$F_{\text{wet}} = C_{\text{VWM}} \times P \quad (2)$$

In the above equations,  $C_{\text{VWM}}$  ( $\mu\text{mol L}^{-1}$ ) is the VWM concentration;  $C_i$  ( $\mu\text{mol L}^{-1}$ ) and  $P_i$  (mm) are the measured N+N or  $\text{NH}_4^+$  concentrations and amount of precipitation during each individual precipitation event, respectively;  $n$  is the number of the precipitation events;  $F_{\text{wet}}$  is the wet deposition flux;  $P$  (mm) is the amount of precipitation.

To demonstrate monthly variability, we calculated monthly wet deposition fluxes ( $\text{mmol m}^{-2} \text{mon}^{-1}$ ) by using the calculated VWM N+N or  $\text{NH}_4^+$  concentration and precipitation amount during each month from May 2014 to January 2015, as rainwater sampling was continuous over this period. In addition, we calculated the annual deposition fluxes by di-

viding a year into two seasons (wet season and dry season). For convenience of discussion, we defined June to November as the wet season ( $>115$  mm rainfall per month), and December to May as the dry season ( $<105$  mm rainfall per month), based on precipitation levels. Each half-year (dry or wet season) wet deposition flux ( $\text{mmol m}^{-2} (\text{half-year})^{-1}$ ) was based on the calculated VWM N+N or  $\text{NH}_4^+$  concentration for that season during the sampling period and the average amount of precipitation during each season over three years (January 2013–December 2015). The annual wet N+N or  $\text{NH}_4^+$  deposition flux was determined as the sum of the wet and dry seasons.

#### 2.4.2 Dry deposition estimates

The dry deposition flux of  $\text{NO}_3^-$  or  $\text{NH}_4^+$  is estimated as the product of the aerosol  $\text{NO}_3^-$  or  $\text{NH}_4^+$  concentration and the deposition velocity, as expressed by eq. (3) (Carbo et al., 2005; Qi et al., 2013; Spokes et al., 2000).

$$F_{\text{dry}} = C_a \times V_d \times (t - t_p) / M, \quad (3)$$

where  $F_{\text{dry}}$  ( $\text{mmol m}^{-2} \text{mon}^{-1}$  or  $\text{mmol m}^{-2} (\text{half year})^{-1}$ ) is the monthly or half-year dry deposition flux;  $C_a$  ( $\mu\text{g m}^{-3}$ ) is the aerosol  $\text{NO}_3^-$  or  $\text{NH}_4^+$  concentration;  $V_d$  ( $\text{cm s}^{-1}$ ) is the deposition velocity;  $t$  (s) is the deposition duration;  $t_p$  (s) is the precipitation duration;  $M$  ( $\text{g mol}^{-1}$ ) is the relative molecular mass of  $\text{NO}_3^-$  or  $\text{NH}_4^+$ .

### 3. Results and discussion

#### 3.1 Precipitation measurements and rainwater DIN concentrations from Yongxing Island

The monthly average precipitation and rainfall duration from Yongxing Island during 2013 to 2015 are shown in Figure 2. Precipitations were more abundant from July–September (with a range of 207.8–319.8 mm) than from January–March (with a range of 1.7–12.8 mm). Monthly average rainfall duration showed a similar pattern as precipitation amount, with durations ranging from 4 to 98 h. Longer rainfall durations were found during months with higher overall amounts of precipitation, except for August and December. Additionally, the precipitation in April was higher than that in May. Generally, higher amounts of precipitation and longer rainfall durations occurred more frequently during the wet season.

Rainwater N+N concentrations ranged from below the detection limit to  $130.9 \mu\text{mol L}^{-1}$  and were dominated by  $\text{NO}_3^-$  (only 3 samples with  $\text{NO}_2^-/(\text{N+N})$  ratio exceeded 2%);  $\text{NH}_4^+$  concentrations ranged from below the detection limit to  $50.9 \mu\text{mol L}^{-1}$ , and recorded precipitation amounts ranged from 0.7 to 134.8 mm. Generally, the rainwater N+N and

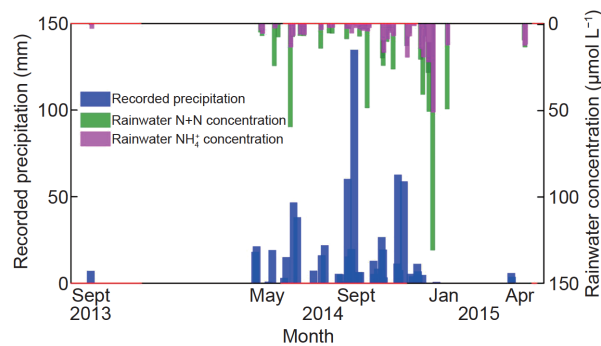


**Figure 2** Precipitation and rainwater concentrations of N+N and  $\text{NH}_4^+$  on Yongxing Island. Red and black color in the x axis represent wet and dry seasons, respectively.

$\text{NH}_4^+$  concentrations were lower during the wet seasons and relatively higher during dry seasons. Comparing between N+N and  $\text{NH}_4^+$ ,  $\text{NH}_4^+$  concentrations were generally lower than those of N+N, especially in dry seasons. The lowest N+N concentrations were found in August, September and November of 2014. Low  $\text{NH}_4^+$  concentrations occurred in May, September, October and November. Both N+N and  $\text{NH}_4^+$  concentrations increased to their maxima in December of 2014. Recorded precipitation reached its maximum in September of 2014 and a minimum in January of 2015 (Figure 3). Generally, the rainwater N+N and  $\text{NH}_4^+$  concentrations showed reverse seasonal variations compared to precipitation amount (N+N:  $r=-0.31$ ,  $p=0.05$ ;  $\text{NH}_4^+$ :  $r=-0.25$ ,  $p=0.13>0.05$ ). Lower concentrations of N+N and  $\text{NH}_4^+$  in rainwater found during the wet seasons are likely due to a dilution effect by rainfall during atmospheric transport from the source regions (Qiao et al., 2015; Xiao et al., 2017).

The VWM rainwater N+N concentration was  $4.9 \mu\text{mol L}^{-1}$  in the wet season and  $18.1 \mu\text{mol L}^{-1}$  in the dry season, and the annual average was  $6.8 \mu\text{mol L}^{-1}$ . The VWM rainwater  $\text{NH}_4^+$  concentration was  $4.3 \mu\text{mol L}^{-1}$  in the wet season and  $9.4 \mu\text{mol L}^{-1}$  in the dry season, with  $5.0 \mu\text{mol L}^{-1}$  as the

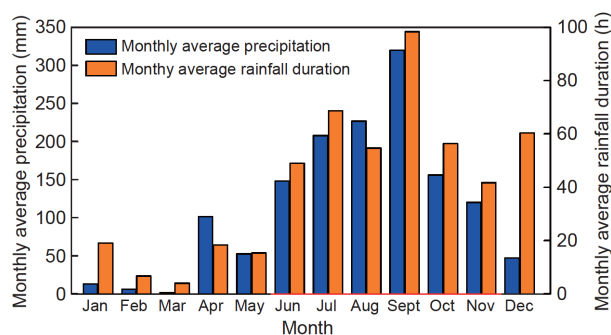


**Figure 3** Monthly average precipitation and rainfall duration from 2013–2015. Red and black color in the x axis represent wet and dry seasons, respectively.

annual average. The VWM rainwater N+N concentration we measured in the dry season was higher than the value of  $14.6 \mu\text{mol L}^{-1}$  over the southern SCS in December 2013, while the VWM  $\text{NH}_4^+$  concentration was only a quarter of that reported by Cui et al. (2016) (Table 1).

The annual VWM rainwater N+N ( $6.8 \mu\text{mol L}^{-1}$ ) and  $\text{NH}_4^+$  ( $5.0 \mu\text{mol L}^{-1}$ ) concentrations over the SCS are significantly lower than over other coastal seas. For example, the annual VWM N+N and  $\text{NH}_4^+$  concentrations were 63.4 and  $107.1 \mu\text{mol L}^{-1}$  over Jiaozhou Bay (in the Yellow Sea, Xing et al., 2017), 70.0 (only  $\text{NO}_3^-$ ) and  $50.0 \mu\text{mol L}^{-1}$  over the northeastern Mediterranean coast (Al-Momani et al., 1995), and  $\sim 40$  and  $\sim 2.1 \mu\text{mol L}^{-1}$  over the east coast of Korea (Park et al., 2019). This is reasonable as our sampling site (the open northwestern SCS) is relatively distant from land, and anthropogenic influences may be expected to be less severe compared to in the Yellow Sea, the Mediterranean coast off Turkey or the east coast of Korea. In contrast, our observed N+N and  $\text{NH}_4^+$  concentrations are similar to or higher than those from the open ocean. The annual average  $\text{NO}_3^-$  and  $\text{NH}_4^+$  concentrations were found to be 5.3 and  $5.2 \mu\text{mol L}^{-1}$  in the Atlantic Ocean at  $50^\circ\text{N}$ – $50^\circ\text{S}$  (Baker et al., 2010) and 0.9 and  $1.5 \mu\text{mol L}^{-1}$  in the open western Pacific (Martino et al., 2014). This finding suggests that the marginal seas have relatively more influence from the continents, in terms of atmospheric N deposition, than the open ocean.

### 3.2 Aerosol $\text{NO}_3^-$ concentrations over the SCS

The aerosol  $\text{NO}_3^-$  concentrations over the SCS during June of 2017 ranged from 0.33 to  $5.54 \mu\text{g m}^{-3}$  ( $1.15 \pm 1.18 \mu\text{g m}^{-3}$  in average). The highest value was found in the southern SCS, and the lowest value in the northern SCS at  $14^\circ\text{N}$  (Figure 4). Wind direction and back trajectories of air masses showed that southwest and southeast winds over the SCS prevailed during the cruise (Figures 5 and 6), which may have carried

the pollutants from Southeast Asia into the southern SCS. This result is consistent with literature reports that the SCS receives considerable quantities of polluted air masses from Southeast Asia during wet seasons (Atwood et al., 2013; Geng et al., 2019; Song et al., 2018; Xiao et al., 2017). Distance from the continent of the Southeast Asia may have determined the aerosol concentrations collected in the SCS during the wet season; this assumption is supported by the atmospheric back trajectory results, and that in the 2 main transects (from the southern SCS to the northern SCS shelf, and from the central SCS to the northern SCS shelf), the aerosol  $\text{NO}_3^-$  concentrations decreased northward.

Table 2 compares our measured aerosol  $\text{NO}_3^-$  concentration with those reported in the literature. In the SCS, the average concentration observed during the wet season ( $1.15 \pm 1.18 \mu\text{g m}^{-3}$ ) is similar to previous results from Yongxing Island during the wet seasons of 2014–2015 ( $1.30 \pm 0.64 \mu\text{g m}^{-3}$ , Xiao et al., 2017). It is also comparable to the concentration of  $1.43 \pm 0.68 \mu\text{g m}^{-3}$  observed in the summer of 2016 and  $1.33 \pm 0.70 \mu\text{g m}^{-3}$  in the summer of 2017 over the western Taiwan Strait/northeastern SCS (Wu et al., 2019). However, it is higher than the  $0.58 \mu\text{g m}^{-3}$  measured over the western SCS during August–September of 2014 (Song et al., 2018), and the  $\sim 0.54 \mu\text{g m}^{-3}$  measured over Daya Bay (in the northern SCS) during the wet seasons of 2015–2017 (Wu et al., 2018). Our observed concentrations is lower than the  $\sim 2.80 \mu\text{g m}^{-3}$  found over Dongsha Island (on the northern SCS shelf) during the wet seasons of 2017–2019 (Chen and Huang, 2018). Compared with the wet seasons of other coastal areas, our observed concentrations is higher than the  $0.47 \pm 0.10 \mu\text{g m}^{-3}$  found over the Arabian Sea (Bange et al., 2000), but lower than the  $1.73 \mu\text{g m}^{-3}$  found over the East Sea (Park et al., 2019) and  $2.13 \mu\text{g m}^{-3}$  over the East China Sea (Nakamura et al., 2005).

The aerosol  $\text{NO}_3^-$  and  $\text{NH}_4^+$  concentrations found over many marginal seas, including the SCS, generally show similar seasonal variations, with higher values during dry

**Table 1** Comparison of rainwater N+N and  $\text{NH}_4^+$  concentrations<sup>a)</sup>

| Locations   | N+N<br>( $\mu\text{mol L}^{-1}$ ) | $\text{NH}_4^+$<br>( $\mu\text{mol L}^{-1}$ ) | Sampling periods  | Note                                   | Data source            |
|---|-----------------------------------|---|---|--|------------------------|
| Yongxing Island (northwestern SCS)                      | 4.9<br>18.1                       | 4.3<br>9.4                                    | Sept. 2013; May 2014 to<br>Jan. 2015; Apr. 2015                             | VWM of wet season<br>VWM of dry season | This study             |
| Southern SCS  | 14.6                              | 41.4  | Dec. 2013   | Individual value                       | Cui et al., 2016       |
| Jiaozhou Bay (Yellow Sea)                               | 63.4                              | 107.1   | Jun. 2015 to May 2016   | VWM                                    | Xing et al., 2017      |
| Northeastern Mediterranean coast of Turkey              | 70.0*                             | 50.0  | Dec. 1991 to Dec. 1992  | VWM                                    | Al-Momani et al., 1995 |
| East coast of Korea (East Sea)                          | $\sim 36.8$                       | $\sim 2.1$                                    | Mar. 2014 to Feb. 2016  | VWM                                    | Park et al., 2019      |
| $50^\circ\text{N}$ – $50^\circ\text{S}$ of the Atlantic | 5.3*                              | $\sim 5.2$                                    | 2000 to 2005  | VWM                                    | Baker et al., 2010     |
| Open Northwestern Pacific                               | 0.9*                              | 1.5   | May and Jun. 2007; Apr.,<br>May, Aug. and Sept. 2008;<br>Oct. and Nov. 2009 | –                                      | Martino et al., 2014   |

a) \*,  $\text{NO}_3^-$  concentration

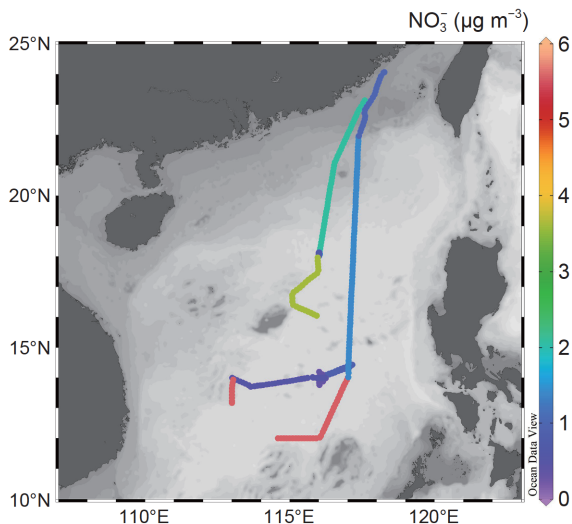


**Figure 4** Aerosol  $\text{NO}_3^-$  concentrations over the SCS during the June 2017 cruise. Each color line represents one sample or several neighboring samples.

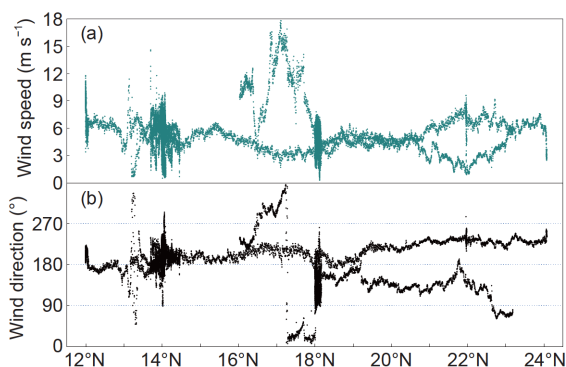


**Figure 5** Wind speeds and directions during the June 2017 cruise. (a) Wind speed ( $\text{m s}^{-1}$ ); (b) wind direction, 0 is a North wind; 90 is an East wind; 180 is a South wind; 270 is a West wind.

seasons and lower values during wet seasons (Bange et al., 2000; Chen and Huang, 2018; Park et al., 2019; Wu et al., 2019; Wu et al., 2018; Xiao et al., 2015, 2017). Anthropogenic particles produced by fossil fuel burning in eastern China and biomass burning in Sumatra and Borneo are the dominant source of fine particles in aerosols over the SCS during the northeast monsoon (dry season) and the southwest monsoon (wet season), respectively (Lin et al., 2007; Xiao et al., 2015). These facts indicate that the pollutants from northeastern Asia have a great impact on the SCS. The dominant source of  $\text{NO}_3^-$  to the SCS is secondary inorganic aerosols from fossil fuel combustion (especially coal combustion in northern Asia), accounting for 69.5%, and the dominant sources of  $\text{NH}_4^+$  are oceanic emission and biomass combustion (Chen and Huang, 2018; Xiao et al., 2017). The low aerosol  $\text{NO}_3^-$  concentrations during the wet seasons may be due to higher temperatures which are more favorable for the evaporation of ammonium nitrate ( $\text{NH}_4\text{NO}_3(\text{s}) \rightleftharpoons \text{NH}_3(\text{g})$

+ $\text{HNO}_3(\text{g})$ , Bai et al., 1995), the prevailing southwesterly winds which carry relatively clean air masses from over the open ocean (Wu et al., 2019), and effective removal by precipitation.

### 3.3 Seasonal variability of wet and dry DIN deposition

Monthly wet deposition fluxes of  $\text{N}+\text{N}$  and  $\text{NH}_4^+$  ranged from 0.4–3.9 and 0.2–1.3  $\text{mmol m}^{-2} \text{mon}^{-1}$ , showing no conspicuous seasonal patterns. Maximum and minimum monthly fluxes occurred in July and May 2014, respectively (Figure 7). During the dry seasons, wet deposition fluxes of  $\text{N}+\text{N}$  and  $\text{NH}_4^+$  were mainly related to rainfall duration rather than precipitation or rainwater concentrations. In the wet seasons, due to the sufficient rainfall, wet deposition fluxes were primarily a function of rainwater concentrations ( $F_{\text{wet}}(\text{N}+\text{N})$  vs.  $\text{VWM}(\text{N}+\text{N})$ ):  $r=0.85$ ,  $p<0.05$ .

We used eq. (3) to estimate the dry deposition fluxes of  $\text{NO}_3^-$  and  $\text{NH}_4^+$ , which are based on the atmospheric concentration ( $C_a$ ) and the aerosol deposition velocity ( $V_d$ ). The deposition velocity ( $V_d$ ) is influenced by several processes, such as gravitational settling, impaction, and diffusion of particles to the water (Duce et al., 1991; Jickells and Spokes, 2001), all which happen simultaneously. Since it is affected by wind speed, particle size, relative humidity, air viscosity, sea surface roughness, and the air/water temperature difference,  $V_d$  is difficult to calculate or measure. Usually  $V_d$  is obtained by models, such as a two-layer model (Duce et al., 1991; Qi et al., 2005; Williams, 1982) or a Chemical Mass Balance Deposition Model (Caffrey et al., 1998).

In general,  $\text{NO}_3^-$  is predominant in coarse particles, whereas  $\text{NH}_4^+$  is often predominant in fine particles (Boreddy and Kawamura, 2015; Fu et al., 2018; Hoppel, 2002; Li et al., 2013; Xiao et al., 2015), causing a higher  $V_d$  for  $\text{NO}_3^-$  than  $\text{NH}_4^+$ . Moreover,  $V_d$  increases with increasing wind speed, with overall higher values during dry than wet seasons (Qi et al., 2005). Table 3 lists the  $V_d$  values adopted in the literature, which range from 0.87–1.7  $\text{cm s}^{-1}$  for  $\text{NO}_3^-$  and 0.05–1.0  $\text{cm s}^{-1}$  for  $\text{NH}_4^+$ . In order to estimate the dry deposition flux of DIN to the SCS, we thus used values of 1.0 and 1.2  $\text{cm s}^{-1}$  for  $\text{NO}_3^-$ , and 0.5 and 0.6  $\text{cm s}^{-1}$  for  $\text{NH}_4^+$ , during the wet and dry seasons, respectively.

Although we only have wet season aerosol  $\text{NO}_3^-$  measurements from one cruise, our results are highly consistent with other studies conducted in the open SCS (on Yongxing Island) during the wet season. We thus used the data collected in June 2017 ( $1.15 \mu\text{g m}^{-3}$ ) to represent aerosol  $\text{NO}_3^-$  concentrations during the wet season. As no cruise samples were collected during the dry season, we thus took the result of  $2.43 \mu\text{g m}^{-3}$  measured on Yongxing Island by Xiao et al.

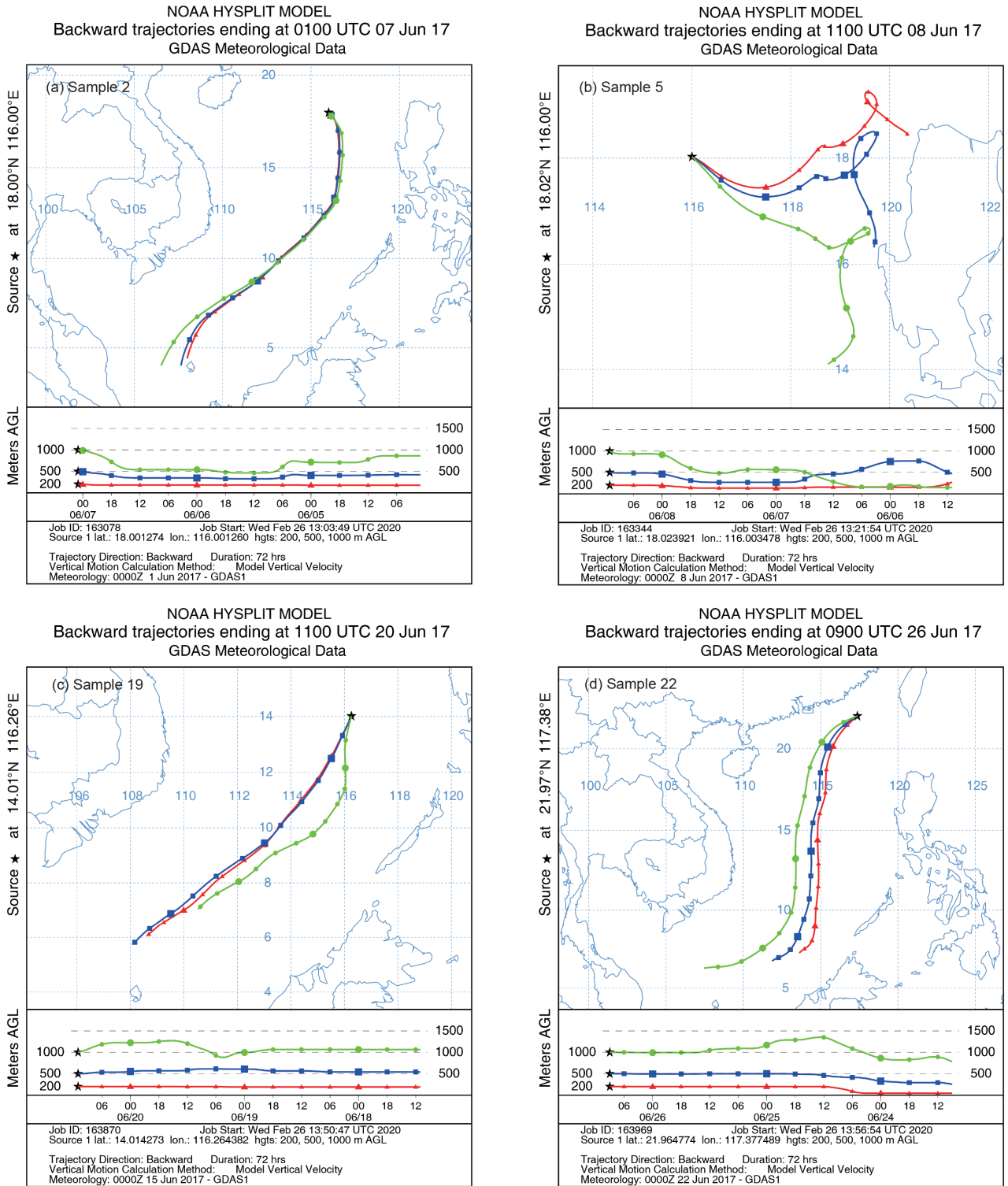


**Figure 6** Back trajectories of samples 2, 5, 19 and 22. (a) Sample 2 is the representative of samples 1–4; (b) sample 5 of samples 5–8; (c) sample 19 of samples 9–21, owing to their parallel back trajectories; (d) back trajectories of sample 22. The figure was drawn with HYSPLIT: The Hybrid Single-Particle Lagrangian Integrated Trajectory. Maryland: NOAA Air Resources Laboratory.

(2017) to represent  $\text{NO}_3^-$  concentrations during the dry season. We have no measurement of aerosol  $\text{NH}_4^+$ , which has been found to be ~3% of the aerosol concentration of  $\text{NO}_3^-$  on

Yongxing Island (aerosol  $\text{NH}_4^+$  concentrations of  $0.04 \mu\text{g m}^{-3}$  during the wet season and  $0.08 \mu\text{g m}^{-3}$  during the dry season, Xiao et al., 2017). Considering the comparable  $\text{NO}_3^-$  results

**Table 2** Comparison of aerosol  $\text{NO}_3^-$  and  $\text{NH}_4^+$  concentrations in the marginal seas and open oceans

|                | Locations                          | $\text{NO}_3^-$<br>( $\mu\text{g m}^{-3}$ ) | $\text{NH}_4^+$<br>( $\mu\text{g m}^{-3}$ ) | Sampling periods  | Data source           |
|----------------|------------------------------------|---|---|---|-----------------------|
|                | SCS                                | 1.15  | –   | Jun. 2017   | This study            |
|                | Yongxing Island (northwestern SCS) | $1.30 \pm 0.64^*$                           | 0.04  | Wet seasons of Mar. 2014 to Feb. 2015                                 | Xiao et al., 2017     |
|                | Yongxing Island                    | $1.69^{**}$                                 | –   | Wet seasons of Mar. 2013 to Jan. 2014                                 | Xiao et al., 2015     |
|                | Western Taiwan Strait              | $1.43 \pm 0.68$                             | $0.72 \pm 0.38$                             | Jul. and Aug. 2016  | Wu et al., 2019       |
|                | Western Taiwan Strait              | $1.33 \pm 0.70$                             | $0.73 \pm 0.56$                             | Jul. and Aug. 2017  | Wu et al., 2019       |
| Wet season     | Western SCS                        | 0.58  | 0.30  | Aug. to Sept. 2014  | Song et al., 2018     |
|                | Daya Bay (northern SCS)            | $\sim 0.54^\dagger$                         | $0.08^\dagger$                              | Sept. 2015; Apr. to Sept. 2016  | Wu et al., 2018       |
|                | Dongsha Island (northern SCS)      | $\sim 2.80^\dagger$                         | $1.19^\dagger$                              | Jun. to Nov. 2007; Jun. to Nov. 2008                                  | Chen and Huang, 2018  |
|                | Arabian Sea                        | $0.47 \pm 0.10$                             | $0.05 \pm 0.03$                             | Jul., Aug. 1995   | Bange et al., 2000    |
|                | East Sea                           | 1.73  | 1.80  | Summer of 2014 to 2016  | Park et al., 2019     |
|                | East China Sea                     | 2.13  | 2.96  | Sept. to Oct. 2002  | Nakamura et al., 2005 |
|                | Yongxing Island, SCS               | $2.43 \pm 1.54^*$                           | 0.08  | Dry seasons of Mar. 2014 to Feb. 2015                                 | Xiao et al., 2017     |
|                | Yongxing Island, SCS               | $2.80^{**}$                                 | –   | Dry seasons of Mar. 2013 to Jan. 2014                                 | Xiao et al., 2015     |
|                | Northern SCS                       | 8.53  | 3.42  | Jan. 2003   | Zhang et al., 2007    |
|                | Northern SCS                       | $1.08 \pm 0.55$                             | $0.15 \pm 0.07$                             | Nov. 2004; Jan. 2005  | Hsu et al., 2007      |
|                | SCS                                | $3.93 \pm 2.01$                             | $4.02 \pm 2.17$                             | Jan. and Feb. 2010  | He, 2011              |
| Dry season     | Dongsha Island, SCS                | $\sim 3.93^\dagger$                         | $1.64^\dagger$                              | Apr., May 2007; Dec. 2007 to May 2008; Dec. 2008 to Mar. 2009         | Chen and Huang, 2018  |
|                | Daya Bay, SCS                      | $\sim 0.64^\dagger$                         | $0.08^\dagger$                              | Oct. 2015 to Mar. 2016; Oct. 2016 to Mar. 2017                        | Wu et al., 2018       |
|                | North Bay of Bengal                | 0.99  | 3.78  | Jan. 2009   | Srinivas et al., 2011 |
|                | Arabian Sea                        | $1.32 \pm 0.39$                             | $0.34 \pm 0.18$                             | May 1995  | Bange et al., 2000    |
|                | East Sea                           | 4.30  | 1.90  | Winter of 2014 to 2016  | Park et al., 2019     |
| Annual average | Open Northwestern Pacific          | 0.18  | 0.13  | May and Jun. 2007; Apr., May, Aug. and Sept. 2008; Oct. and Nov. 2009 | Martino et al., 2014  |

a) \*, Jun. to Sept. as the wet seasons; Mar., Apr., Oct., Nov., Dec. 2014 and Jan., Feb. 2015 as the dry seasons; \*\*, May to Aug. 2013 as the wet season; Mar. 2013, Oct. 2013 to Jan. 2014 as the dry seasons; † approximate values, recalculated based on the data reported in the references; -: No data

between our data collected in the SCS basin and the data collected on Yongxing Island by Xiao et al. (2017), we adopted their aerosol  $\text{NH}_4^+$  concentrations to estimate the dry deposition of  $\text{NH}_4^+$  to the SCS.

The calculated monthly dry deposition rates ranged from  $0.4\text{--}1.2 \text{ mmol m}^{-2} \text{ mon}^{-1}$  for  $\text{NO}_3^-$  and  $0.01\text{--}0.02 \text{ mmol m}^{-2} \text{ mon}^{-1}$  for  $\text{NH}_4^+$  (Table 4) with the higher fluxes occurring during the dry season. Dry deposition fluxes are related to aerosol concentrations,  $V_d$  and the duration between precipitation events.

The monthly wet and dry DIN fluxes to the SCS ranged from  $0.6\text{--}4.8$  and  $0.4\text{--}1.2 \text{ mmol m}^{-2} \text{ mon}^{-1}$ , respectively (Table 4). The ratio of monthly dry deposition to monthly total deposition varied from 8.9% to 67.1%, with the highest and lowest ratios observed in May and July 2014, respectively (Figure 8). Annually, the wet deposition flux accounted for 62.5% of total DIN deposition to the SCS. The dominance of wet DIN deposition over the SCS in this study is consistent with other studies from the SCS, most other of the marginal seas and the open oceans. For example, Yang et

al. (2014) report a DIN wet deposition to total deposition ratio of 66.7%. This ratio was 54.7% in the northwestern Pacific (Martino et al., 2014), 83.5% in the North Sea (modeled result from Hertel et al., 2002), 71.3–80% in the Yellow Sea (Qi et al., 2013), and 78.2% in the Atlantic at  $50^\circ\text{N}\text{--}50^\circ\text{S}$  (Baker et al., 2010).

In the air over the SCS,  $\text{NO}_3^-$  is mainly a secondary particle formed from condensable atmospheric gases (including water vapor and initially volatile gases after photochemical oxidation) (Kolb and Worsnop, 2012; Xiao et al., 2017). The mechanism of  $\text{NO}_3^-$  formation from condensable atmospheric gases simultaneously causes ultrafine particles to grow via coagulation and increases the overall particle size. Particles of size  $0.1\text{--}1.0 \mu\text{m}$  will be removed efficiently by precipitation (Al-Momani et al., 1995). Along with this mechanism, more rainfall increases wet deposition flux; cleaner air masses from the southwest lower dry deposition flux, which may result in higher wet than dry deposition rates during the wet season. During the dry season, as a result of less precipitation, shorter rainfall durations, more polluted air masses and higher  $V_d$ , the proportion of dry deposition to

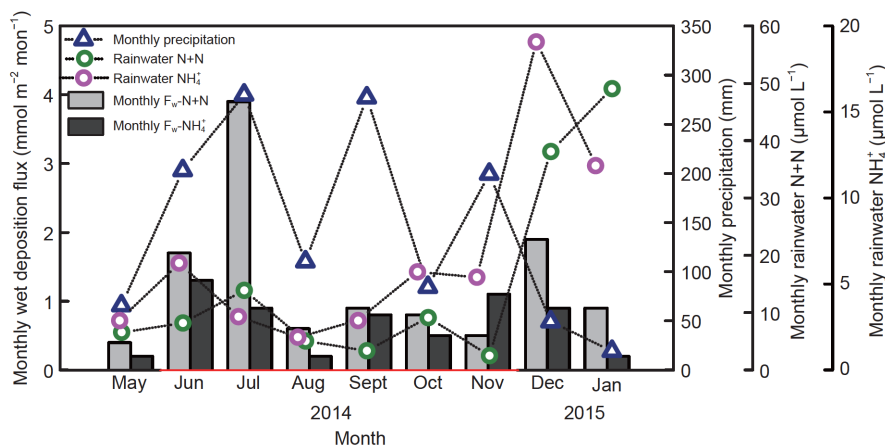


**Figure 7** Monthly precipitation, rainwater N+N and  $\text{NH}_4^+$  concentrations and wet deposition fluxes of N+N and  $\text{NH}_4^+$  from May 2014 to January 2015. Red and black color in the x axis represent wet and dry seasons, respectively.

**Table 3** Deposition velocity ( $V_d$ ) of  $\text{NO}_3^-$  and  $\text{NH}_4^+$  reported in the literature

| Locations   | $V_d$ of $\text{NO}_3^-$<br>( $\text{cm s}^{-1}$ ) | $V_d$ of $\text{NH}_4^+$<br>( $\text{cm s}^{-1}$ ) | Sampling periods                          | Season         | References           |
|---|--|--|---|----------------|----------------------|
| Dongsha Island (northern SCS)                       | 1.2  | 0.1  | Apr. 2007 to Mar. 2009                    | Annual average | Chen and Huang, 2018 |
| Western Taiwan Strait (Northern SCS)                | 1.15   | 0.6  | 2016 to 2017                              | Annual average | Wu et al., 2019      |
| East China Sea                                      | 1.2  | 0.1  | Apr., Jul., Nov. and Dec. 2010; Mar. 2011 | Annual average | Li et al., 2013      |
| Jiaozhou Bay (Yellow Sea)                           | 0.26   | 0.09   | Spring of 2016                            | Spring         | Xing et al., 2018    |
|   | 0.37   | 0.10   | Summer of 2015                            | Summer         | Xing et al., 2018    |
|   | 0.54   | 0.25   | Autumn of 2015                            | Autumn         | Xing et al., 2018    |
|   | 0.23   | 0.24   | Winter of 2015                            | Winter         | Xing et al., 2018    |
| Yellow Sea  | 1.15   | 0.5  | 1997 to 2005                              | Annual average | Zhang et al., 2011   |
| Arabian Sea   | 1.5  | 0.05   | May, Jul. and Aug. 1995; Mar. 1997        | Annual average | Bange et al., 2000   |
| East Sea  | 1.7  | 0.22   | Mar. 2014 to Feb. 2016                    | Annual average | Park et al., 2019    |
| Remote western North Pacific                        | 0.87   | 1.0  | Mar. to Apr. 2014                         | Dry season     | Fu et al., 2018      |
| Coastal Levantine basin (eastern Mediterranean Sea) | 1.2  | 0.6  | Jan. 2001 to Apr. 2003                    | Annual average | Carbo et al., 2005   |
| Mace Head Ireland (eastern Atlantic)                | 1.15   | 0.6  | Jun. 1996; May 1997                       | Wet season     | Spokes et al., 2000  |

the total flux increased.

### 3.4 Annual wet and dry deposition of DIN

The wet deposition fluxes during the wet and dry seasons were estimated to be 5.7 and 4.0  $\text{mmol m}^{-2}$  (half year) $^{-1}$  for N+N, and 5.0 and 2.1  $\text{mmol m}^{-2}$  (half year) $^{-1}$  for  $\text{NH}_4^+$ , respectively. The annual wet DIN deposition flux was 16.8  $\text{mmol m}^{-2} \text{yr}^{-1}$  (Table 4), lower than those previously reported at Dongsha Island on the northern SCS shelf ( $32 \pm 40 \text{mmol m}^{-2} \text{yr}^{-1}$ , Yang et al., 2014), the East Sea ( $31\text{--}51 \text{mmol m}^{-2} \text{yr}^{-1}$ , Park et al., 2019), the North Sea ( $37.0 \text{mmol m}^{-2} \text{yr}^{-1}$ , modeled result from Hertel et al., 2002), and Jiaozhou Bay in the Yellow Sea ( $147.7 \text{mmol m}^{-2} \text{yr}^{-1}$ , Xing et al., 2017) (Table 5). However,

it is higher than values reported in the Arabian Sea ( $10.6 \text{mmol m}^{-2} \text{yr}^{-1}$ , Bange et al., 2000), the northwestern Pacific ( $3.5 \text{mmol m}^{-2} \text{yr}^{-1}$ , Martino et al., 2014) and from  $50^\circ\text{N}\text{--}50^\circ\text{S}$  in the Atlantic ( $9.3 \text{mmol m}^{-2} \text{yr}^{-1}$ , Baker et al., 2010) as shown in Table 5.

The dry deposition fluxes during wet and dry seasons were estimated to be 2.7 and 7.2  $\text{mmol m}^{-2}$  (half year) $^{-1}$  for  $\text{NO}_3^-$ , and 0.05 and 0.1  $\text{mmol m}^{-2}$  (half year) $^{-1}$  for  $\text{NH}_4^+$ . Subsequently, annual dry DIN deposition in the SCS was estimated to be  $10.1 \text{mmol m}^{-2} \text{yr}^{-1}$  (Table 4), similar to the values measured in Daya Bay ( $9.4 \text{mmol m}^{-2} \text{yr}^{-1}$ , Wu et al., 2018) in the northern SCS, the Bay of Bengal ( $9.9 \pm 7.3 \text{mmol m}^{-2} \text{yr}^{-1}$ , Srinivas et al., 2011) and the Arabian Sea ( $12.2 \text{mmol m}^{-2} \text{yr}^{-1}$ , Bange et al., 2000), but lower than values found in the East China Sea ( $41.4 \text{mmol m}^{-2} \text{yr}^{-1}$ , Li

**Table 4** Estimated atmospheric DIN deposition to the SCS<sup>a)</sup>

| Monthly or annual deposition | Time       | N+N              |                  | NH <sub>4</sub> <sup>+</sup> |                  | DIN              |                  | Total DIN flux                  |
|------------------------------|------------|------------------|------------------|------------------------------|------------------|------------------|------------------|---------------------------------|
|                              |            | $F_{\text{wet}}$ | $F_{\text{dry}}$ | $F_{\text{wet}}$             | $F_{\text{dry}}$ | $F_{\text{wet}}$ | $F_{\text{dry}}$ | $F_{\text{wet}}+F_{\text{dry}}$ |
| Monthly deposition           | May 2014   | 0.4              | 1.2              | 0.2                          | 0.02             | 0.6              | 1.2              | 1.8                             |
|                              | Jun. 2014  | 1.7              | 0.4              | 1.3                          | 0.01             | 3.0              | 0.4              | 3.4                             |
|                              | Jul. 2014  | 3.9              | 0.5              | 0.9                          | 0.01             | 4.8              | 0.5              | 5.3                             |
|                              | Aug. 2014  | 0.6              | 0.5              | 0.2                          | 0.01             | 0.8              | 0.5              | 1.3                             |
|                              | Sept. 2014 | 0.9              | 0.4              | 0.8                          | 0.01             | 1.7              | 0.4              | 2.1                             |
|                              | Oct. 2014  | 0.8              | 0.5              | 0.5                          | 0.01             | 1.3              | 0.5              | 1.8                             |
|                              | Nov. 2014  | 0.5              | 0.5              | 1.1                          | 0.01             | 1.6              | 0.5              | 2.1                             |
|                              | Dec. 2014  | 1.9              | 1.1              | 0.9                          | 0.02             | 2.8              | 1.2              | 4.0                             |
|                              | Jan. 2015  | 0.9              | 1.2              | 0.2                          | 0.02             | 1.1              | 1.2              | 2.3                             |
| Annual deposition            | Wet season | 5.7              | 2.7              | 5.0                          | 0.1              | 10.7             | 2.8              | 13.5                            |
|                              | Dry season | 4.0              | 7.2              | 2.1                          | 0.1              | 6.1              | 7.3              | 13.4                            |
|                              | Annual     | 9.7              | 9.9              | 7.1                          | 0.2              | 16.8             | 10.1             | 26.9                            |

a) unit:  $\text{mmol m}^{-2} \text{mon}^{-1}$  for the monthly flux,  $\text{mmol m}^{-2} (\text{half-year})^{-1}$  for the seasonal flux, and  $\text{mmol m}^{-2} \text{yr}^{-1}$  for the annual flux

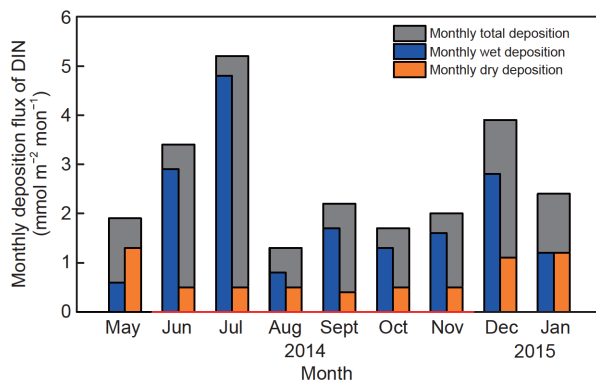


**Figure 8** Monthly wet, dry and total deposition fluxes of N+N and NH<sub>4</sub><sup>+</sup> from May 2014 to January 2015. Red and black color in the x axis represent wet and dry seasons, respectively.

et al., 2013), the coastal Levantine basin (eastern Mediterranean sea,  $56 \text{ mmol m}^{-2} \text{yr}^{-1}$ , Carbo et al., 2005), the East Sea ( $33\text{--}38 \text{ mmol m}^{-2} \text{yr}^{-1}$ , Park et al., 2019), Dongsha Island ( $23\pm 13 \text{ mmol m}^{-2} \text{yr}^{-1}$ , Chen and Huang, 2018;  $16\pm 30 \text{ mmol m}^{-2} \text{yr}^{-1}$ , Yang et al., 2014), and Jiaozhou Bay ( $59.4 \text{ mmol m}^{-2} \text{yr}^{-1}$ , Xing et al., 2018). Finally, the annual dry deposition flux is higher than in the North Sea ( $6.4 \text{ mmol m}^{-2} \text{yr}^{-1}$ , modeled result from Hertel et al., 2002), the Northwestern Pacific ( $2.9 \text{ mmol m}^{-2} \text{yr}^{-1}$ , Martino et al., 2014) and from  $50^{\circ}\text{N}\text{--}50^{\circ}\text{S}$  in the Atlantic ( $2.6 \text{ mmol m}^{-2} \text{yr}^{-1}$ , Baker et al., 2010), as shown in Table 5.

Annually, the total atmospheric deposition flux of DIN in the SCS ( $26.9 \text{ mmol m}^{-2} \text{yr}^{-1}$ ) is larger than in the open ocean, such as in the North Pacific and Atlantic ( $6.4\text{--}11.9 \text{ mmol m}^{-2} \text{yr}^{-1}$ , Baker et al., 2010; Martino et al., 2014), attributed to the fact that marginal seas are more affected by anthropogenic emissions from continents than the open ocean. The SCS total atmospheric DIN flux is com-

parable to that observed in the Arabian Sea ( $22.8 \text{ mmol m}^{-2} \text{yr}^{-1}$ , Bange et al., 2000), but less than those observed in the western Baltic Sea ( $39.7 \text{ mmol m}^{-2} \text{yr}^{-1}$ , Rolff et al., 2008), the North Sea ( $43.4 \text{ mmol m}^{-2} \text{yr}^{-1}$ , Hertel et al., 2002), the East China Sea ( $41.4 \text{ mmol m}^{-2} \text{yr}^{-1}$  of dry deposition, Li et al., 2013), the Yellow Sea ( $50\text{--}70 \text{ mmol m}^{-2} \text{yr}^{-1}$ , modeled result from Zhang et al., 2011), the East Sea ( $64\text{--}89 \text{ mmol m}^{-2} \text{yr}^{-1}$ , Park et al., 2019) and the coastal eastern Mediterranean Sea ( $56 \text{ mmol m}^{-2} \text{yr}^{-1}$  of dry deposition, Carbo et al., 2005) (Table 5).

### 3.5 Potential importance of atmospheric DIN deposition to the SCS

The high temperatures and strong stratification of the surface SCS are favorable for N<sub>2</sub>-fixing organisms. N<sub>2</sub> fixation rates in the SCS show large spatial and temporal variations, with documented values of  $\sim 1.2\pm 0.5$  to  $12.6\pm 5.7 \mu\text{mol N m}^{-2} \text{d}^{-1}$  (Chen et al., 2008),  $51.7\pm 6.2 \mu\text{mol N m}^{-2} \text{d}^{-1}$  (Chen et al., 2014), and  $14.1\pm 12.0$  to  $84.5\pm 76.3 \mu\text{mol N m}^{-2} \text{d}^{-1}$  (Voss et al., 2006). The atmospheric DIN deposition flux ( $26.9 \text{ mmol N m}^{-2} \text{yr}^{-1}$  or  $73.7 \mu\text{mol N m}^{-2} \text{d}^{-1}$ ) is comparable to or higher than the reported N<sub>2</sub> fixation rates.

As one of the external supplies of nutrients to the SCS, the annual atmospheric deposition flux of DIN (both wet and dry,  $26.9 \text{ mmol m}^{-2} \text{yr}^{-1}$ ), when extrapolated to the entire SCS (area of  $3.5\times 10^6 \text{ km}^2$ ), suggesting a total atmospheric DIN flux of  $94.2 \text{ Gmol N yr}^{-1}$ . For comparison, riverine DIN inputs from the Mekong River (NO<sub>3</sub><sup>-</sup>), Pearl River (DIN) and Red River (DIN) are 20, 40 and  $7.7 \text{ Gmol N yr}^{-1}$ , respectively (Grosse et al., 2010; Le et al., 2010; Liu et al., 2009). Therefore, atmospheric DIN deposition can provide a similar magnitude of DIN as compared to the total amount of these large river inputs.

**Table 5** Wet and dry deposition fluxes of N+N, NH<sub>4</sub><sup>+</sup> and DIN in the SCS compared with those reported in previous studies<sup>a)</sup>

| Locations   | N+N              |                  | NH <sub>4</sub> <sup>+</sup> |                  | DIN              |                  | Sampling periods  | Type     | Data source           |
|---|------------------|------------------|------------------------------|------------------|------------------|------------------|---|----------|-----------------------|
|   | F <sub>wet</sub> | F <sub>dry</sub> | F <sub>wet</sub>             | F <sub>dry</sub> | F <sub>wet</sub> | F <sub>dry</sub> |   |          |                       |
| Yongxing Island (SCS)                               | 9.7              | –                | 7.1                          | –                | 16.8             | –                | Sept. 2013; May 2014 to Jan. 2015; Apr. 2015                          | Observed | This study            |
| SCS basin   | –                | 9.9              | –                            | 0.2              | –                | 10.1             | Jun. 2017   | Observed | This study            |
| Dongsha Island, SCS                                 | –                | 21±11            | –                            | 2.5±2.1          | –                | 23±13            | Apr. 2007 to Mar. 2009  | Observed | Chen and Huang, 2018  |
| Dongsha Island, SCS                                 | 15±20*           | 11±26            | 17±20                        | 5±4              | 32±40            | 16±30            | Jul., Sept., Nov. and Dec. 2010; Feb. and Mar. 2011                   | Observed | Yang et al., 2014     |
| Daya Bay, SCS                                       | –                | 8.5*             | –                            | 0.9              | –                | 9.4              | Sept. 2015 to Mar. 2017   | Observed | Wu et al., 2018       |
| the Bay of Bengal                                   | –                | –                | –                            | –                | –                | 9.9±7.3          | Jan. 2009   | Observed | Srinivas et al., 2011 |
| East China Sea                                      | –                | 37.0*            | –                            | 4.4              | –                | 41.4             | Apr., Jul., Nov. and Dec. 2010; Mar. 2011                             | Observed | Li et al., 2013       |
| Coastal Levantine basin (eastern Mediterranean Sea) | –                | 40               | –                            | 16               | –                | 56               | Jan. 2001 to Apr. 2003  | Observed | Carbo et al., 2005    |
| Arabian Sea   | 5.3              | 11.6             | 5.3                          | 0.6              | 10.6             | 12.2             | May, Jul. and Aug. 1995; Mar. 1997                                    | Observed | Bange et al., 2000    |
| Yellow Sea  | 10–20            | 5–10             | 30                           | 5–10             | 40–50            | 10–20            | 1997 to 2005  | Modeled  | Zhang et al., 2011    |
| East Sea  | 17–24            | 27–30            | 14–27                        | 6–8              | 31–51            | 33–38            | Mar. 2014 to Feb. 2016  | Observed | Park et al., 2019     |
| Jiaozhou Bay, Yellow Sea                            | –                | 30.0             | –                            | 29.4             | –                | 59.4             | Jun. 2015 to May 2016   | Observed | Xing et al., 2018     |
| Jiaozhou Bay, Yellow Sea                            | 54.9             | –                | 92.8                         | –                | 147.7            | –                | 2015 to 2016  | Observed | Xing et al., 2017     |
| Western Baltic Sea                                  | –                | 20.8**           | –                            | 18.9**           | –                | 39.7**           | Jul. 2001 to Jun. 2002  | Observed | Rolff et al., 2008    |
| North Sea   | 19.4*            | 3.2*             | 17.6                         | 3.2              | 37.0             | 6.4              | 1999  | Modeled  | Hertel et al., 2002   |
| Northwestern Pacific                                | 1.3*             | 1.6*             | 2.2                          | 1.3              | 3.5              | 2.9              | May and Jun. 2007; Apr., May, Aug. and Sept. 2008; Oct. and Nov. 2009 | Observed | Martino et al., 2014  |
| Remote western North Pacific                        | –                | 5.4*             | –                            | 39.4             | –                | 44.8             | Mar. to Apr. 2014   | Observed | Fu et al., 2018       |
| 50°N–50°S of the Atlantic                           | 5.3*             | 2.2*             | 4.0                          | 0.4              | 9.3              | 2.6              | 2000 to 2005  | Observed | Baker et al., 2010    |

a) \*, Flux of only NO<sub>3</sub><sup>-</sup>; \*\*, seasonal average. unit: mmol m<sup>-2</sup> yr<sup>-1</sup>

Using a C/N ratio of 106:16 (Redfield ratio, Redfield et al., 1963), potentially 5.86 mg C m<sup>-2</sup> d<sup>-1</sup> of new production can be supported by atmospheric DIN deposition. Based on <sup>15</sup>N uptake, new production has been estimated to range from 80 ±10 to 250±140 mg C m<sup>-2</sup> d<sup>-1</sup> in the northern SCS basin and 60±10 to 340±70 in the shelf-slope region. Estimates of total primary production, based on <sup>13</sup>C uptake, ranged from 340 ±130 to 620±70 mg C m<sup>-2</sup> d<sup>-1</sup> in the basin, and 820±40 to 870±260 mg C m<sup>-2</sup> d<sup>-1</sup> in the shelf-slope region (Chen and Chen, 2006; Chen et al., 2007, 2008). Primary production in the whole SCS basin, as derived from SeaWiFS data, is estimated to be 354 mg C m<sup>-2</sup> d<sup>-1</sup> (Liu et al., 2002). In the southern SCS, export production, as estimated by a <sup>228</sup>Ra/NO<sub>3</sub><sup>-</sup> two-source diffusion model, is 52.8 mg C m<sup>-2</sup> d<sup>-1</sup> (Cai et al., 2002). Therefore, atmospheric DIN deposition contributes potentially 1.8–11.1% of the nitrogen supporting new production and 0.7–1.8% of nitrogen supporting total primary production in the SCS.

Comparing these results more broadly, in previous studies based on field sampling, the total atmospheric deposition of N<sub>r</sub> was estimated to potentially contribute 5.6–8.7% of the nitrogen supporting total primary production in the SCS

(Chen and Huang, 2018). Our estimate here is lower than their result, the latter of which includes organic nitrogen deposition. Total atmospheric deposition of DIN has been found to contribute ~1.9% of the nitrogen supporting primary production in the coastal areas east of the Korean Peninsula and in the East Asian marginal seas (Park et al., 2019). N deposition supports 0.3–6.7% (TN) and 1.1–3.9% (TIN) of primary production in the Yellow Sea and the East China Sea (Qi et al., 2013; Zhang et al., 2010), respectively. Atmospheric DIN deposition potentially contributes ~2–15% of the nitrogen supporting primary productivity in the southern North Sea (Spokes and Jickells, 2005). The potential contribution of atmospheric DIN deposition to marine productivity in the SCS is slightly lower than that in the Yellow Sea or East China Sea, and much lower than in the southern North Sea. At the global scale, the atmospheric deposition of NO<sub>y</sub> and NH<sub>y</sub> supports ~0.5% of primary production and ~2.3% of new production in the open ocean (Carr et al., 2006; Duce et al., 2008; Ducklow, 1995; Laws et al., 2000; Oschlies, 2001). The relative importance of atmospheric DIN deposition to SCS productivity is higher than for the global open ocean.

#### 4. Concluding remarks

The annual wet deposition fluxes of N+N and  $\text{NH}_4^+$ , estimated based on rainwater concentrations and amount of precipitation, were 9.7 and 7.1  $\text{mmol m}^{-2} \text{yr}^{-1}$ , respectively, with higher deposition rates found during the wet season than the dry season. Estimated annual dry deposition fluxes of  $\text{NO}_3^-$  and  $\text{NH}_4^+$ , based on large-volume total suspended aerosol particle sampling, were 9.9 and 0.2  $\text{mmol m}^{-2} \text{yr}^{-1}$ , respectively. Annually, wet deposition supplied larger amount of DIN to the SCS compared to the dry pathways (16.8 vs. 10.1  $\text{mmol m}^{-2} \text{yr}^{-1}$ ). The annual atmospheric DIN deposition was estimated as 26.9  $\text{mmol m}^{-2} \text{yr}^{-1}$ , which is higher than or similar to the new nitrogen added to the euphotic zone through  $\text{N}_2$  fixation. The total atmospheric DIN deposition flux to the SCS was 94.2  $\text{Gmol yr}^{-1}$ , comparable to large riverine inputs, and potentially contributes 1.8–11.1% of the nitrogen to new production and 0.7–1.8% of the nitrogen to primary production, which is slightly lower than in the Yellow Sea and East China Sea but slightly higher than the global average. Our findings highlight the influence of human activities on marine biogeochemistry and productivity.

**Acknowledgements** *The Meteorological Bureau of Sansha is appreciated for the rainwater sampling on Yongxing Island. The Meteorological Bureau of Hainan Province provided the precipitation data (amount and duration) from Yongxing Island during 2013–2015. We are grateful to the crew of the R/V Jiageng (TKK) for their help during the cruise (KK1702). Zhentong Yao, Xibao Su, Tao Huang, Ligu Guo, Junhui Chen and Chunlan Liu are appreciated for their help in the rainwater nutrient measurements, preparation of the cruise and aerosol sample processing. We thank Dr. Jinyu Yang's valuable comments which helped to improve the manuscript. We also appreciate the constructive comments and suggestions from three anonymous reviewers, which have improved the quality of this paper. Dr. Richard W. Smith is appreciated for polishing the English. The authors declare that the study was conducted in the absence of any commercial or financial relationships that could be construed as a potential conflict of interest. This study was supported by the National Basic R & D Program of China (Grant No. 2015CB954001) and the National Natural Science Foundation of China (Grant No. 41876080).*

#### References

- Al-Momani I F, Tuncel S, Eler Ü, Örtel E, Sirin G, Tuncel G. 1995. Major ion composition of wet and dry deposition in the eastern Mediterranean basin. *Sci Total Environ*, 164: 75–85
- Atwood S A, Reid J S, Kreidenweis S M, Cliff S S, Zhao Y, Lin N H, Tsay S C, Chu Y C, Westphal D L. 2013. Size resolved measurements of springtime aerosol particles over the northern South China Sea. *Atmos Environ*, 78: 134–143
- Bai H, Lu C, Ling Y M. 1995. A theoretical study on the evaporation of dry ammonium chloride and ammonium nitrate aerosols. *Atmos Environ*, 29: 313–321
- Baker A R, Lesworth T, Adams C, Jickells T D, Ganzeveld L. 2010. Estimation of atmospheric nutrient inputs to the Atlantic Ocean from 50°N to 50°S based on large-scale field sampling: Fixed nitrogen and dry deposition of phosphorus. *Glob Biogeochem Cycle*, 24: GB3006
- Bange H W, Rixen T, Johansen A M, Siefert R L, Ramesh R, Ittekkot V, Hoffmann M R, Andreae M O. 2000. A revised nitrogen budget for the Arabian Sea. *Glob Biogeochem Cycle*, 14: 1283–1297
- Boreddy S K R, Kawamura K. 2015. A 12 year observation of water-soluble inorganic ions in TSP aerosols collected at a remote marine location in the western North Pacific: An outflow region of Asian dust. *Atmos Chem Phys Discuss*, 15: 7419–7458
- Caffrey P F, Ondov J M, Zufall M J, Davidson C I. 1998. Determination of size-dependent dry particle deposition velocities with multiple intrinsic elemental tracers. *Environ Sci Technol*, 32: 1615–1622
- Cai P, Huang Y, Chen M, Guo L, Liu G, Qiu Y. 2002. New production based on  $^{228}\text{Ra}$ -derived nutrient budgets and thorium-estimated POC export at the intercalibration station in the South China Sea. *Deep Sea Res Part I-Oceanogr Res Pap*, 49: 53–66
- Carbo P, Krom M D, Homoky W B, Benning L G, Herut B. 2005. Impact of atmospheric deposition on N and P geochemistry in the southeastern Levantine basin. *Deep Sea Res Part II-Top Stud Oceanogr*, 52: 3041–3053
- Carr M E, Friedrichs M A M, Schmeltz M, Noguchi Aita M, Antoine D, Arrigo K R, Asanuma I, Aumont O, Barber R, Behrenfeld M, Bidigare R, Buitenhuis E T, Campbell J, Ciotti A, Dierssen H, Dowell M, Dunne J, Esaias W, Gentili B, Gregg W, Groom S, Hoepffner N, Ishizaka J, Kameda T, Le Quéré C, Lohrenz S, Marra J, Mélin F, Moore K, Morel A, Reddy T E, Ryan J, Scardi M, Smyth T, Turpie K, Tilstone G, Waters K, Yamanaka Y. 2006. A comparison of global estimates of marine primary production from ocean color. *Deep Sea Res Part II-Top Stud Oceanogr*, 53: 741–770
- Chen C T A, Wang S L, Wang B J, Pai S C. 2001. Nutrient budgets for the South China Sea basin. *Mar Chem*, 75: 281–300
- Chen H Y, Huang S Z. 2018. Effects of atmospheric dry deposition on external nitrogen supply and new production in the northern South China Sea. *Atmosphere*, 9: 386
- Chen Y L, Chen H Y, Lin Y H, Yong T C, Taniuchi Y, Tuo S. 2014. The relative contributions of unicellular and filamentous diazotrophs to  $\text{N}_2$  fixation in the South China Sea and the upstream Kuroshio. *Deep Sea Res Part I-Oceanogr Res Pap*, 85: 56–71
- Chen Y L, Chen H Y, Tuo S, Ohki K. 2008. Seasonal dynamics of new production from Trichodesmium  $\text{N}_2$  fixation and nitrate uptake in the upstream Kuroshio and South China Sea basin. *Limnol Oceanogr*, 53: 1705–1721
- Chen Y L, Chen H Y. 2006. Seasonal dynamics of primary and new production in the northern South China Sea: The significance of river discharge and nutrient advection. *Deep Sea Res Part I-Oceanogr Res Pap*, 53: 971–986
- Chen Y, Mills S, Street J, Golan D, Post A, Jacobson M, Paytan A. 2007. Estimates of atmospheric dry deposition and associated input of nutrients to Gulf of Aqaba seawater. *J Geophys Res*, 112: D04309
- Cui D Y, Wang J T, Tan L J, Dong Z Y. 2016. Impact of atmospheric wet deposition on phytoplankton community structure in the South China Sea. *Estuar Coast Shelf Sci*, 173: 1–8
- Dentener F, Drevet J, Lamarque J F, Bey I, Eickhout B, Fiore A M, Hauglustaine D, Horowitz L W, Krol M, Kulshrestha U C, Lawrence M, Galy-Lacaux C, Rast S, Shindell D, Stevenson D, Van Noije T, Atherton C, Bell N, Bergman D, Butler T, Cofala J, Collins B, Doherty R, Ellingsen K, Galloway J, Gauss M, Montanaro V, Müller J F, Pitari G, Rodriguez J, Sanderson M, Solmon F, Strahan S, Schultz M, Sudo K, Szopa S, Wild O. 2006. Nitrogen and sulfur deposition on regional and global scales: A multimodel evaluation. *Glob Biogeochem Cycle*, 20: GB4003
- Duce R. 1986. *The Role of Air-sea Exchange in Geochemical Cycling*. Dordrecht: Springer. 497–529
- Duce R A, LaRoche J, Altieri K, Arrigo K R, Baker A R, Capone D G, Cornell S, Dentener F, Galloway J, Ganeshram R S, Geider R J, Jickells T, Kuypers M M, Langlois R, Liss P S, Liu S M, Middelburg J J, Moore C M, Nickovic S, Oschlies A, Pedersen T, Prospero J, Schlitzer R, Seitzinger S, Sorensen L L, Uematsu M, Ulloa O, Voss M, Ward B, Zamora L. 2008. Impacts of atmospheric anthropogenic nitrogen on the open ocean. *Science*, 320: 893–897

- Duce R A, Liss P S, Merrill J T, Atlas E L, Buat-Menard P, Hicks B B, Miller J M, Prospero J M, Arimoto R, Church T M, Ellis W, Galloway J N, Hansen L, Jickells T D, Knap A H, Reinhardt K H, Schneider B, Soudine A, Tokos J J, Tsunogai S, Wollast R, Zhou M. 1991. The atmospheric input of trace species to the world ocean. *Glob Biogeochem Cycle*, 5: 193–259
- Ducklow H W. 1995. Ocean biogeochemical fluxes: New production and export of organic matter from the upper ocean. *Rev Geophys*, 33: 1271–1276
- Fowler D, Coyle M, Skiba U, Sutton M A, Cape J N, Reis S, Sheppard L J, Jenkins A, Grizzetti B, Galloway J N, Vitousek P, Leach A, Bouwman A F, Butterbach-Bahl K, Dentener F, Stevenson D, Amann M, Voss M. 2013. The global nitrogen cycle in the twenty-first century. *Phil Trans R Soc B*, 368: 20130164
- Fu J, Wang B, Chen Y, Ma Q. 2018. The influence of continental air masses on the aerosols and nutrients deposition over the western North Pacific. *Atmos Environ*, 172: 1–11
- Galloway J N, Cowling E B. 2002. Reactive nitrogen and the world: 200 years of change. *AMBIO-A J Human Environ*, 31: 64–71
- Geng X, Zhong G, Li J, Cheng Z, Mo Y, Mao S, Su T, Jiang H, Ni K, Zhang G. 2019. Molecular marker study of aerosols in the northern South China Sea: Impact of atmospheric outflow from the Indo-China Peninsula and South China. *Atmos Environ*, 206: 225–236
- Grosse J, Bombar D, Doan H N, Nguyen L N, Voss M. 2010. The Mekong River plume fuels nitrogen fixation and determines phytoplankton species distribution in the South China Sea during low and high discharge season. *Limnol Oceanogr*, 55: 1668–1680
- Han A, Dai M H, Kao S J, Gan J P, Li Q, Wang L F, Zhai W D, Wang L. 2012. Nutrient dynamics and biological consumption in a large continental shelf system under the influence of both a river plume and coastal upwelling. *Limnol Oceanogr*, 57: 486–502
- He Y H. 2011. Composition and sources of water soluble ions in atmosphere aerosol water soluble ions over the China coastal seas (in Chinese). Dissertation for Master's Degree. Qingdao: Ocean University of China
- Hertel O, Ambelas Skjøth C, Frohn L M, Vignati E, Frydendall J, de Leeuw G, Schwarz U, Reis S. 2002. Assessment of the atmospheric nitrogen and sulphur inputs into the North Sea using a Lagrangian model. *Phys Chem Earth Parts A/B/C*, 27: 1507–1515
- Hoppel W A. 2002. Surface source function for sea-salt aerosol and aerosol dry deposition to the ocean surface. *J Geophys Res-Oceans*, 107: 4382, doi: 10.1029/2001jd002014
- Hsu S C, Lee C S L, Huh C A, Shaheen R, Lin F J, Liu S C, Liang M C, Tao J. 2014. Ammonium deficiency caused by heterogeneous reactions during a super Asian dust episode. *J Geophys Res-Atmos*, 119: 6803–6817
- Hsu S C, Liu S C, Kao S J, Jeng W L, Huang Y T, Tseng C M, Tsai F, Tu J Y, Yang Y. 2007. Water-soluble species in the marine aerosol from the northern South China Sea: High chloride depletion related to air pollution. *J Geophys Res*, 112: D19304
- Jickells T, Spokes L. 2001. *The Biogeochemistry of Iron in Seawater*. Chichester: John Wiley & Sons Ltd. 85–121
- Kanakidou M, Myriokefalitakis S, Tsagkaraki M. 2020. Atmospheric inputs of nutrients to the Mediterranean Sea. *Deep Sea Res Part II-Top Stud Oceanogr*, 171: 104606, doi: 10.1016/j.dsr2.2019. 06.014
- Karl D M. 1999. Minireviews: A sea of change: Biogeochemical variability in the North Pacific subtropical gyre. *Ecosystems*, 2: 181–214
- Kim T W, Lee K, Duce R, Liss P. 2014. Impact of atmospheric nitrogen deposition on phytoplankton productivity in the South China Sea. *Geophys Res Lett*, 41: 3156–3162
- Kolb C E, Worsnop D R. 2012. Chemistry and composition of atmospheric aerosol particles. *Annu Rev Phys Chem*, 63: 471–491
- Krishnamurthy A, Moore J K, Zender C S, Luo C. 2007. Effects of atmospheric inorganic nitrogen deposition on ocean biogeochemistry. *J Geophys Res*, 112: G02019
- Laws E A, Falkowski P G, Smith Jr. W O, Ducklow H, McCarthy J J. 2000. Temperature effects on export production in the open ocean. *Glob Biogeochem Cycle*, 14: 1231–1246
- Le T P Q, Gilles B, Garnier J, Sylvain T, Denis R, Anh N X, Minh C V. 2010. Nutrient (N, P, Si) transfers in the subtropical Red River system (China and Vietnam): Modelling and budget of nutrient sources and sinks. *J Asian Earth Sci*, 37: 259–274
- Li Z, Chen Y, Guo L, Wang F. 2013. Estimate of dry deposition fluxes of nutrients over the East China Sea: The implication of aerosol ammonium to non-sea-salt sulfate ratio to nutrient deposition of coastal oceans. *Atmos Environ*, 69: 131–138
- Lin I I, Chen J P, Wong G T F, Huang C W, Lien C C. 2007. Aerosol input to the South China Sea: Results from the MODerate resolution imaging spectro-radiometer, the quick scatterometer, and the measurements of pollution in the troposphere sensor. *Deep Sea Res Part II-Top Stud Oceanogr*, 54: 1589–1601
- Liu K K, Chao S Y, Shaw P T, Gong G C, Chen C C, Tang T Y. 2002. Monsoon-forced chlorophyll distribution and primary production in the South China Sea: Observations and a numerical study. *Deep Sea Res Part I-Oceanogr Res Pap*, 49: 1387–1412
- Liu S M, Hong G H, Zhang J, Ye X W, Jiang X L. 2009. Nutrient budgets for large Chinese estuaries. *Biogeosciences*, 6: 2245–2263
- Ludwig W, Dumont E, Meybeck M, Heussner S. 2009. River discharges of water and nutrients to the Mediterranean and Black Sea: Major drivers for ecosystem changes during past and future decades? *Prog Oceanogr*, 80: 199–217
- Luo L, Yao X H, Gao H W, Hsu S C, Li J W, Kao S J. 2016. Nitrogen speciation in various types of aerosols in spring over the northwestern Pacific Ocean. *Atmos Chem Phys*, 16: 325–341
- Martino M, Hamilton D, Baker A R, Jickells T D, Bromley T, Nojiri Y, Quack B, Boyd P W. 2014. Western Pacific atmospheric nutrient deposition fluxes, their impact on surface ocean productivity. *Glob Biogeochem Cycle*, 28: 712–728
- Millero F J. 2016. *Chemical Oceanography*, 4th ed. Boca Raton: CRC press. 571
- Nakamura T, Matsumoto K, Uematsu M. 2005. Chemical characteristics of aerosols transported from Asia to the East China Sea: An evaluation of anthropogenic combined nitrogen deposition in autumn. *Atmos Environ*, 39: 1749–1758
- Oschlies A. 2001. Model-derived estimates of new production: New results point towards lower values. *Deep Sea Res Part II-Top Stud Oceanogr*, 48: 2173–2197
- Pai S C, Tsau Y J, Yang T I. 2001. PH and buffering capacity problems involved in the determination of ammonia in saline water using the indophenol blue spectrophotometric method. *Anal Chim Acta*, 434: 209–216
- Park G H, Lee S E, Kim Y I, Kim D, Lee K, Kang J, Kim Y H, Kim H, Park S, Kim T W. 2019. Atmospheric deposition of anthropogenic inorganic nitrogen in airborne particles and precipitation in the East Sea in the northwestern Pacific Ocean. *Sci Total Environ*, 681: 400–412
- Prospero J M, Barrett K, Church T, Dentener F, Duce R A, Galloway J N, Levy I H, Moody J, Quinn P. 1996. Atmospheric deposition of nutrients to the North Atlantic Basin. *Biogeochemistry*, 35: 27–73
- Qi J H, Li P, Li X, Feng L, Zhang M. 2005. Estimation of dry deposition fluxes of particulate species to the water surface in the Qingdao area, using a model and surrogate surfaces. *Atmos Environ*, 39: 2081–2088
- Qi J H, Shi J H, Gao H W, Sun Z. 2013. Atmospheric dry and wet deposition of nitrogen species and its implication for primary productivity in coastal region of the Yellow Sea, China. *Atmos Environ*, 81: 600–608
- Qiao X, Xiao W, Jaffe D, Kota S H, Ying Q, Tang Y. 2015. Atmospheric wet deposition of sulfur and nitrogen in Jiuzhaigou National Nature Reserve, Sichuan Province, China. *Sci Total Environ*, 511: 28–36
- Redfield A C, Ketchum B H, Richards F A. 1963. The influence of organisms on the composition of sea-water. *The Sea*, 2: 26–77
- Rolf C, Elmgren R, Voss M. 2008. Deposition of nitrogen and phosphorus on the Baltic Sea: Seasonal patterns and nitrogen isotope composition. *Biogeosciences*, 5: 1657–1667
- Shi J, Gao H, Qi J, Zhang J, Yao X. 2010. Sources, compositions, and distributions of water-soluble organic nitrogen in aerosols over the China Sea. *J Geophys Res*, 115: D17303

- Shiozaki T, Furuya K, Kodama T, Takeda S. 2009. Contribution of  $N_2$  fixation to new production in the western North Pacific Ocean along  $155^\circ E$ . *Mar Ecol Prog Ser*, 377: 19–32
- Song J, Zhao Y, Zhang Y, Fu P, Zheng L, Yuan Q, Wang S, Huang X, Xu W, Cao Z, Gromov S, Lai S. 2018. Influence of biomass burning on atmospheric aerosols over the western South China Sea: Insights from ions, carbonaceous fractions and stable carbon isotope ratios. *Environ Pollution*, 242: 1800–1809
- Spokes L J, Yeatman S G, Cornell S E, Jickells T D. 2000. Nitrogen deposition to the eastern Atlantic Ocean. The importance of south-easterly flow. *Tellus B-Chem Phys Meteorol*, 52: 37–49
- Spokes L J, Jickells T D. 2005. Is the atmosphere really an important source of reactive nitrogen to coastal waters? *Cont Shelf Res*, 25: 2022–2035
- Srinivas B, Sarin M M, Sarma V V S S. 2011. Atmospheric dry deposition of inorganic and organic nitrogen to the Bay of Bengal: Impact of continental outflow. *Mar Chem*, 127: 170–179
- Voss M, Bombar D, Loick N, Dippner J W. 2006. Riverine influence on nitrogen fixation in the upwelling region off Vietnam, South China Sea. *Geophys Res Lett*, 33: L07604
- Wang B, Huang F, Wu Z, Yang J, Fu X, Kikuchi K. 2009. Multi-scale climate variability of the South China Sea monsoon: A review. *Dyn Atmos Oceans*, 47: 15–37
- Wang H, Shi G, Tian M, Chen Y, Qiao B, Zhang L, Yang F, Zhang L, Luo Q. 2018. Wet deposition and sources of inorganic nitrogen in the Three Gorges Reservoir Region, China. *Environ Pollut*, 233: 520–528
- Williams R M. 1982. A model for the dry deposition of particles to natural water surfaces. *Atmos Environ*, 16: 1933–1938
- Wong G T F, Tseng C M, Wen L S, Chung S W. 2007. Nutrient dynamics and N-anomaly at the SEATS station. *Deep Sea Res Part II-Top Stud Oceanogr*, 54: 1528–1545
- Wu S P, Dai L H, Zhu H, Zhang N, Yan J P, Schwab J J, Yuan C S. 2019. The impact of sea-salt aerosols on particulate inorganic nitrogen deposition in the western Taiwan Strait region, China. *Atmos Res*, 228: 68–76
- Wu Y, Zhang J, Liu S, Jiang Z, Huang X. 2018. Aerosol concentrations and atmospheric dry deposition fluxes of nutrients over Daya Bay, South China Sea. *Mar Pollution Bull*, 128: 106–114
- Xiao H W, Xiao H Y, Luo L, Shen C Y, Long A M, Chen L, Long Z H, Li D N. 2017. Atmospheric aerosol compositions over the South China Sea: Temporal variability and source apportionment. *Atmos Chem Phys*, 17: 3199–3214
- Xiao H W, Xie L H, Long A M, Ye F, Pan Y P, Li D N, Long Z H, Chen L, Xiao H Y, Liu C Q. 2015. Use of isotopic compositions of nitrate in TSP to identify sources and chemistry in South China Sea. *Atmos Environ*, 109: 70–78
- Xing J, Song J, Yuan H, Li X, Li N, Duan L, Kang X, Wang Q. 2017. Fluxes, seasonal patterns and sources of various nutrient species (nitrogen, phosphorus and silicon) in atmospheric wet deposition and their ecological effects on Jiaozhou Bay, North China. *Sci Total Environ*, 576: 617–627
- Xing J, Song J, Yuan H, Wang Q, Li X, Li N, Duan L, Qu B. 2018. Water-soluble nitrogen and phosphorus in aerosols and dry deposition in Jiaozhou Bay, North China: Deposition velocities, origins and biogeochemical implications. *Atmos Res*, 207: 90–99
- Yang J Y T, Hsu S C, Dai M H, Hsiao S S Y, Kao S J. 2014. Isotopic composition of water-soluble nitrate in bulk atmospheric deposition at Dongsha Island: Sources and implications of external N supply to the northern South China Sea. *Biogeosciences*, 11: 1833–1846
- Zhang J, Zhang G S, Bi Y F, Liu S M. 2011. Nitrogen species in rainwater and aerosols of the Yellow and East China seas: Effects of the East Asian monsoon and anthropogenic emissions and relevance for the NW Pacific Ocean. *Glob Biogeochem Cycle*, 25: GB3020
- Zhang J J, Li H L, Xuan J L, Wu Z Z, Yang Z, Wiesner M G, Chen J F. 2019. Enhancement of mesopelagic sinking particle fluxes due to upwelling, aerosol deposition, and monsoonal influences in the north-western South China Sea. *J Geophys Res-Oceans*, 124: 99–112
- Zhang X, Lin C, Zhou X, Lei K, Guo B, Cao Y, Lu S, Liu X, He M. 2019. Concentrations, fluxes, and potential sources of nitrogen and phosphorus species in atmospheric wet deposition of the Lake Qinghai Watershed, China. *Sci Total Environ*, 682: 523–531
- Zhang X Y, Zhuang G S, Guo J H, Yin K D, Zhang P. 2007. Characterization of aerosol over the Northern South China Sea during two cruises in 2003. *Atmos Environ*, 41: 7821–7836
- Zhang Y, Yu Q, Ma W C, Chen L M. 2010. Atmospheric deposition of inorganic nitrogen to the eastern China seas and its implications to marine biogeochemistry. *J Geophys Res*, 115: D00K10

(Responsible editor: Chuanlun ZHANG)